Volume 1
Number 2
November 2023
Pages 125-340

RSC Applied Polymers

rsc.li/RSCApplPolym

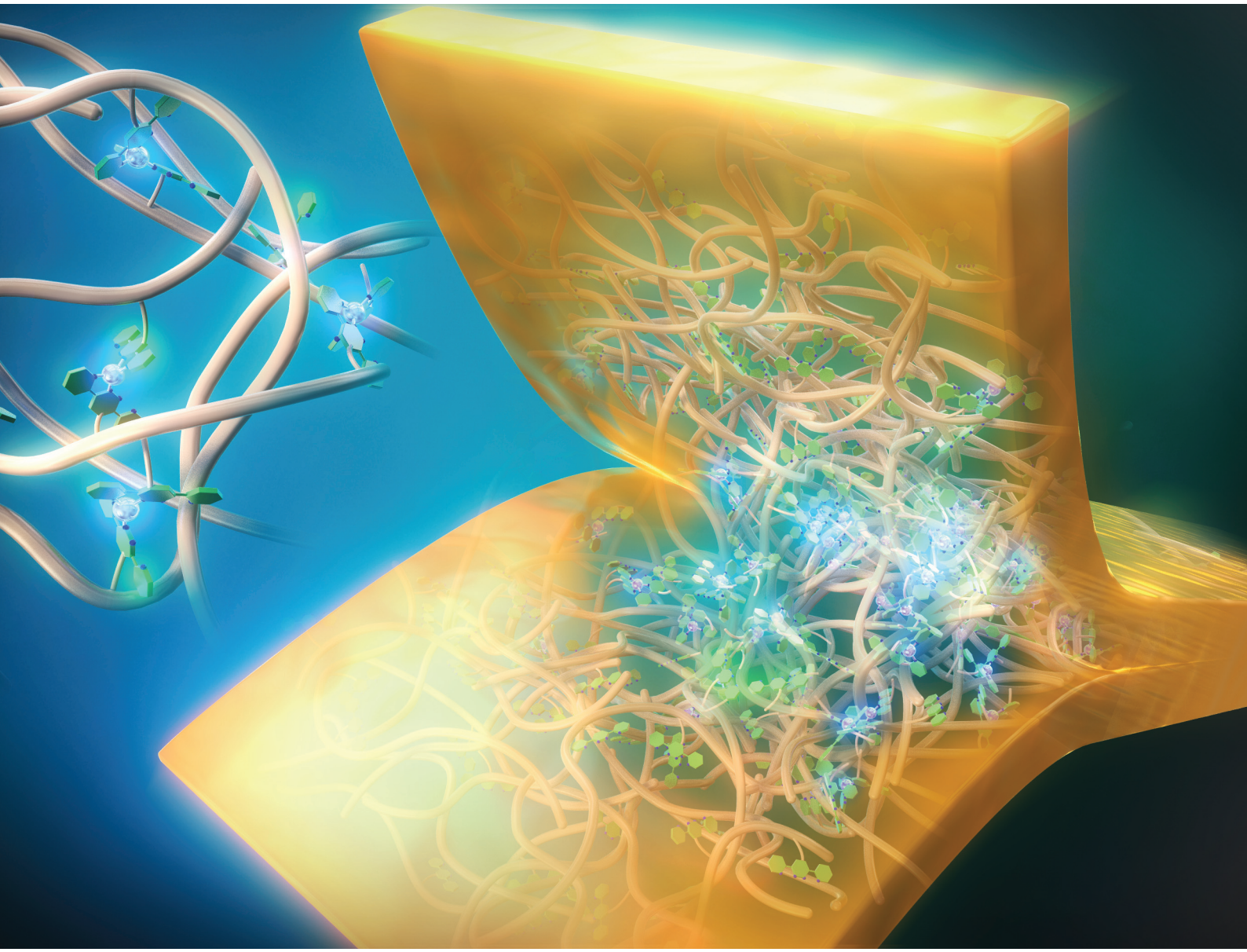

ISSN 2755-371X

ROYAL SOCIETY OF CHEMISTRY

PAPER
Kyohei Kotani *et al.*
Tough tetrazine-functionalized styrene–butadiene rubber with self-adhesion through zinc–nitrogen coordination

RSC Applied Polymers

ROYAL SOCIETY OF CHEMISTRY

PAPER

View Article Online
View Journal | View Issue

Cite this: *RSC Appl. Polym.*, 2023, **1**, 229

Tough tetrazine-functionalized styrene–butadiene rubber with self-adhesion through zinc–nitrogen coordination†

Kyohei Kotani,*[a,b] Katsuhiko Tsunoda[a] and Hideyuki Otsuka *[b]

We report a feasible system for the direct adhesion of cross-linked rubbers, based on incorporating tetrazine ligands into a styrene–butadiene rubber (SBR) followed by the addition of zinc dimethacrylate (ZDMA) with the aim of forming reversible coordination cross-links. The modification of SBR is achieved using an inverse-electron-demand Diels–Alder (IEDDA) click reaction with 3,6-di(2-pyridyl)-1,2,4,5-tetrazine (DPT) during the rubber-kneading process. The complexation capability of the bound DPT in the SBR with ZDMA is demonstrated using a small model molecule including a DPT unit *via* UV-vis spectra. The obtained DPT–ZDMA cross-linked rubbers show unique temperature dependence in dynamic mechanical analysis (DMA), demonstrating the dissociation and reassociation of the DPT–ZDMA cross-linking. Strain-sweep DMA tests exhibited a typical Payne effect with increasing amount of bound DPT units in the SBR, supporting the formation of ZDMA–ZDMA filler interactions. Furthermore, the reversible nature of DPT–ZDMA cross-linking endows the resulting composites with high strength. A tensile strength of up to 30.5 MPa at 579% elongation was achieved when 2.6 mol% of DPT was incorporated into SBR with 40 phr of ZDMA. Hysteresis measurements revealed that the amount of bound DPT in the SBR and the ZDMA content significantly impact the hysteresis loss due to the dissociation of the DPT–ZDMA cross-linking and ZDMA–ZDMA filler interactions, leading to high energy dissipation and high toughness. Finally, a direct adhesion application was demonstrated using T-peel tests, where the adhesion-peeling force reaches up to 5.72 N mm^{-1} when 2.6 mol% of DPT was incorporated into SBR with 60 phr of ZDMA. The maximum peeling force showed a good correlation with the difference between the E' value at 25 °C and that at 145 °C as obtained from the DMA tests, clearly demonstrating that the degree of DPT–ZDMA cross-linking is a main factor in determining the adhesion strength in the DPT–ZDMA cross-linking system.

Received 14th July 2023,
Accepted 11th September 2023

DOI: 10.1039/d3lp00112a

rsc.li/rscapplpolym

Introduction

Adhesion between cross-linked rubbers is one of the most important processes for engineering the manufacture of rubber products.[1] However, it is commonly known that direct adhesion between cross-linked rubbers without treatment of the rubber surfaces is quite difficult due to the restricted polymer-chain mobility on account of cross-linking,[1–5] and therefore, it is not surprising that pretreatment methods for rubber-surface modifications and adhesive technology have been widely studied.[1,6–13] Nonetheless, repair processes, such as tyre retreading, for cured rubber products that involve an adhesion process between cross-linked rubbers are still limited given several issues with the processes, including curing temperature and time.[14–18]

To develop a more efficient adhesion system, it is important to induce the interdiffusion of polymer chains between two cured rubber samples during an adhesion process, such as heat-pressing, followed by interlinkage between the two rubber samples after cooling. Hence, the introduction of reversible linkages,[1,19–22] such as hydrogen bonds,[23–26] ionic interactions,[27–33] host–guest interactions,[34,35] dynamic covalent bonds[36–45] and metal–ligand coordination bonds,[25,46–55] given that introducing cross-linking bonds into cured rubber is a potential strategy to achieve direct adhesion between cross-linked rubbers, as reversible linkages often show a temperature dependence that is different from that of

[a]*Sustainable and Advanced Materials Division, Bridgestone Corporation, 3-1-1, Ogawahigashi-cho, Kodaira-shi, Tokyo 187-8531, Japan.*
E-mail: kyohei.kotani@bridgestone.com
[b]*Department of Chemical Science and Engineering, Tokyo Institute of Technology, 2-12-1 Ookayama, Meguro-ku, Tokyo, 152-8550, Japan.*
E-mail: otsuka@mac.titech.ac.jp

† Electronic supplementary information (ESI) available. See DOI: https://doi.org/10.1039/d3lp00112a

conventional covalent bonds, which results in good malleability at high temperature. Metal–ligand coordination bonds are particularly promising cross-linkages on account of their bonding energy, which can be controlled by changing the type of metal salt and the design of the ligands on the polymer chains. For example, Bao *et al.*[47] have designed a highly stretchable autonomously self-healing poly(dimethylsiloxane) (PDMS) by introducing the 2,6-butylpyridinedicarboxyamide ligand and cross-linking with $FeCl_3$. The resulting cross-linked PDMS samples show a high recovered-fracture strain due to the metal–ligand exchange and the low T_g (below −90 °C) of the PDMS, giving high mobility to the polymer chain. Weder *et al.*[52] have demonstrated that cross-linkages that consist of the 2,6-bis(1′-methylbenzimidazolyl)-pyridine ligand, incorporated into a styrene–butadiene rubber (SBR) *via* a thiol–ene reaction, and $Zn(OTf)_2$ can act as reversible bonds and show a unique tan δ peak at *ca.* 90 °C due to energy dissipation upon activation of the metal–ligand cross-linkages at this temperature in dynamic-mechanical-analysis (DMA) measurements. Das *et al.*[53] have reported that a mixture of epoxidized natural rubber (ENR), $FeCl_3$, zinc acetate dihydrate, and 2,6-diaminopyridine (DAP) forms reversible cross-links and exhibits self-healing behaviour at 60 °C. In this system, Fe^{3+} ions form bonds with the oxygen atom of the epoxy group in the ENR, while DAP not only acts as a catalyst for the ring-opening of the epoxide moiety, but also kinetically controls the release of Fe^{3+}.

Meanwhile, the incorporation of ligand molecules into the conventional rubber polymer chains is of great interest from a manufacturing perspective. One of the most promising methods in this context is click chemistry,[56] which is characterized by high atom-efficiency and performed under relatively mild conditions. In particular, inverse-electron-demand Diels–Alder (IEDDA) reactions between tetrazine moieties and unsaturated bonds[57–60] is a powerful tool to incorporate functional groups into polymer chains.[54,55,61,62] Recently, Wu *et al.* have reported a route for the modification of NBR[54] and SBR[55] using the IEDDA reaction with 3,6-di(2-pyridyl)-1,2,4,5-tetrazine (DPT) during the rubber-mixing process. The resulting polymers form reversible cross-links with metal salts ($ZnCl_2$, $CoCl_2$ and $CuSO_4$), and show self-healing behaviour upon thermal treatment at 170–190 °C. However, the metal salts used in the aforementioned studies are not easy to handle in realistic industrial rubber-mixing processes due to their hygroscopicity and the risks they present to human health and/or the environment. Thus, we were interested to create a more feasible system, especially from the viewpoint of material handling in the rubber industry.

In this study, zinc dimethacrylate (ZDMA) was selected for the formation of the reversible metal–ligand cross-links with DPT-modified SBRs. ZDMA is not hygroscopic and less toxic than the aforementioned metal salts, and is thus widely used in the rubber industry as a reinforcing cross-linking coagent, mainly with peroxide curing systems.[29,31–33,63–68] The objective of this study was to design novel cross-linked SBR composites that exhibit direct adhesion behaviour without the need for pretreatment (Fig. 1). For this purpose, we prepared DPT-modified SBRs using a rubber-kneading process with reference to a previous study,[55] and investigated the coordination capability of the DPT unit towards ZDMA. Subsequently, the DPT-modified SBRs were compounded with ZDMA, which acted not only as a cross-linking agent, but also as a reinforcing filler. Finally, the physical properties of the resulting cross-linked samples, including their dynamic viscoelasticity, tensile behaviour and adhesive strength, were examined in detail. The obtained results demonstrate that the DPT–ZDMA cross-linking network is successfully formed to endow the resulting SBR composites with unique physical properties, including high tensile strength and improved adhesion strength.

Experimental

Materials

A random solution styrene–butadiene copolymer (SBR; 25 wt% styrene and 75 wt% butadiene; grade: TUFDENE™ 2000R) was purchased from Asahi Kasei Corp. Zinc dimethacrylate (ZDMA,

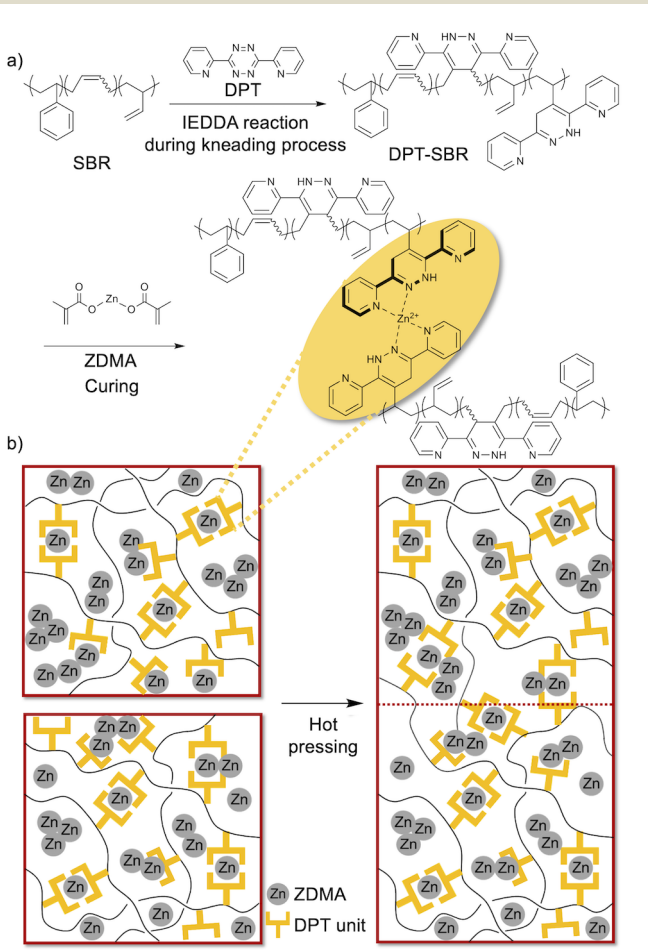

Fig. 1 Conceptual outline of this study: (a) preparation of DPT-modified SBRs by IEDDA reactions during the kneading process, followed by the formation of DPP–ZDMA cross-linkages and (b) schematic description of the adhesion process *via* rearrangement of the DPT–ZDMA cross-linkages.

Dymalink® 708) was obtained from Cray Valley Co., Ltd. Dichloroacetic acid, *cis*-cyclooctene and 3,6-di(2-pyridyl)-1,2,4,5-tetrazine (DPT) were acquired from Tokyo Chemical Industry Co., Ltd. Dicumyl peroxide and chloroform-d_1 were purchased from Sigma Aldrich Co. LLC. Tetrahydrofuran (THF), toluene, dichloromethane, xylene, methanol, *n*-hexane, *n*-heptane and silica gel 60 N (spherical, neutral) were acquired from Kanto Chemical Co., Ltd. 1,1,2,2-Tetrachloroethane-d_2 was purchased from Fujifilm Wako Pure Chemical Corp.

Measurements

Gel-permeation chromatography (GPC) measurements were carried out at 40 °C using a TOSOH HLC-8320 GPC system equipped with a guard column (TOSOH TSK guard column HXL-H), two separation columns (TOSOH TSK gel GMHXL), a differential refractive-index (RI) detector and a UV detector. Tetrahydrofuran (THF) was used as the eluent at a flow rate of 0.6 mL min^{-1}. Polystyrene (PS) standards (M_w = 8 420 000–1010 g mol^{-1}) were used to calibrate the GPC system. Differential-scanning-calorimetry (DSC) measurements were conducted using a DSC2500 (TA Instruments Inc.) instrument under an atmosphere of nitrogen at a heating rate of 20 °C min^{-1}. High-resolution mass spectra (HRMS) were obtained using an Acquity UPLC system coupled to a Xevo G2-XS QTOF mass spectrometer (Waters) using MeOH as the eluent. Fourier-transform infrared (FT-IR) spectra were recorded at room temperature on a Nicolet iS5 FT-IR spectrometer using a germanium-crystal attenuated-total-reflectance (ATR) attachment (Thermo Scientific Inc.). ^{1}H and ^{13}C NMR spectra were measured in chloroform-d_1 ($CDCl_3$) with tetramethylsilane (TMS) as the internal standard or 1,1,2,2-tetrachloroethane-d_2 ($C_2D_2Cl_4$) at 300 K on a Bruker AVANCE III HD 600 MHz spectrometer. UV-vis spectra were measured at room temperature in CH_2Cl_2 using a V-680 (Jasco Corp.) spectrophotometer. Rotorless rheometer measurements were carried out at 145 °C using an RLR-4 (Toyo Seiki Manufacturing Co. Ltd) instrument under a pressure of 10 MPa with a fixed amplitude angle of ±1° and a frequency of 100 cpm. Dynamic mechanical analysis (DMA) tests were conducted on a GABO EPLEXOR (Netzsch) apparatus equipped with a 500 N load cell, using standard JIS-K6251 strip-shaped specimens (length: 40.0 mm; width: 4.7 mm). Temperature-sweep DMA tests were carried out under tensile mode with a fixed frequency of 15 Hz, a static strain of 6%, a dynamic strain of 0.4%, and a heating rate of 2 °C min^{-1} from −75 to 150 °C. The strain-sweep tests were conducted at 25 °C under tensile mode with a fixed frequency of 15 Hz, a static strain of 10%, and a dynamic strain range from 0.1 to 10%. Tensile tests were carried out at room temperature using an Instron 5965 (Instron) instrument equipped with a 5 kN load cell at a crosshead speed of 100 mm min^{-1}, using dumbbell-shaped ISO 37-4 specimens. Three measurements were performed for each sample. The fracture energy, W, was calculated using the equation $W = \int_0^{\varepsilon} \sigma(\varepsilon)\mathrm{d}\varepsilon$. Hysteresis tests were performed at room temperature using an Instron 5965 (Instron) apparatus equipped with a 5 kN load cell at a crosshead speed of 100 mm min^{-1}, using dumbbell-shaped ISO 37-4 specimens. The hysteresis loss was calculated using the equation, Hysteresis loss = $W_{stored} - W_{unload}$, where $W_{stored}(\varepsilon) = \int_0^{\varepsilon} \sigma(\varepsilon')\mathrm{d}\varepsilon'$ and W_{unload} were calculated using the stress–strain relationship for the unloading process. T-peel adhesion tests were conducted at room temperature on an Instron 5965 (Instron) instrument equipped with a 5 kN load cell at a crosshead speed of 300 mm min^{-1} using laminated stripes (length: 75 mm; width: 10 mm). Two measurements were performed for each sample.

Preparation of DPT-modified SBRs

SBR (65.0 g) and varying amounts of DPT were kneaded at 70 rpm at 120 °C for 3 min in an internal mixer (Toyo Seiki Manufacturing Co. Ltd). The resulting DPT–SBRs were denoted as DPT–SBR1, DPT–SBR2 and DPT–SBR3, for DPT loading amounts of 1, 2 and 4 mol% relative to the butadiene unit in the SBR, respectively.

Synthesis of DPT-CO[57]

A round-bottom flask was charged with 3,6-di(2-pyridyl)-1,2,4,5-tetrazine (0.472 g, 2.00 mmol) and xylene (20 mL), before the resulting solution was sparged with nitrogen gas. Subsequently, *cis*-cyclooctene (0.331 g, 3.00 mmol) was added to the solution, which was subsequently stirred under reflux conditions at a setting temperature of 160 °C. After 20 min, the red solution turned pale yellow, indicating that the reaction had reached completion. The solution was then concentrated under reduced pressure, before the thus obtained residue was subjected to column chromatography on silica gel using acetone/*n*-hexane 5/95 (v/v) to give 0.612 g (1.92 mmol, 96%) of DPT-CO as a yellow solid. ^{1}H NMR ($CDCl_3$, 600 MHz, δ): 8.81 (s, 1H), 8.63 (ddd, J = 4.8, 1.7, 1.1 Hz, 1H), 8.59 (ddd, J = 4.8, 1.7, 1.1 Hz, 1H), 8.08 (dt, J = 8.0, 1.0 Hz, 1H), 7.72 (td, J = 7.7, 1.4 Hz, 1H), 7.63 (m, 1H), 7.54 (m, 1H), 7.21 (ddd, J = 7.5, 4.8, 1.0 Hz, 1H), 7.16 (ddd, J = 7.4, 4.8, 1.1 Hz, 1H), 4.40 (m, 1H), 2.90 (ddd, J = 15.2, 9.0, 3.3 Hz, 1H), 2.15 (m, 1H), 2.07 (m, 1H), 1.88 (m, 1H), 1.83–1.65 (m, 5H), 1.63–1.56 (m, 2H), 1.53 (m, 1H). ^{13}C NMR ($CDCl_3$, 150 MHz, δ): 154.8, 152.6, 149.4, 148.6, 143.2, 136.3, 135.8, 133.8, 124.0, 122.5, 122.4, 121.0, 112.4, 35.3, 31.4, 28.8, 27.6, 26.9, 24.7, 22.8. IR (ATR, cm^{-1}) 3265, 2917, 2860, 1580, 1564, 1488, 1471, 1427, 1353, 1152. HRMS (ESI) [M + Na] calcd for $C_{20}H_{22}N_4Na$ 341.1742; found 341.1790. UV-vis (6.4×10^{-5} M in CH_2Cl_2, nm) λ_{max} 255, 325.

Mixing and curing conditions for the uncured rubber samples

SBR or DPT–SBRs (15 g, 100 phr) were mixed with different amounts of ZDMA for 10 min on a two-roll open mill with a roller speed of 15 rpm at 65 °C. The SBR/ZDMA mixtures were further mixed with varying amount of dicumyl peroxide (DCP) for 2 min on the two-roll open mill with a roller speed of 15 rpm at 65 °C. The resulting samples were hot-pressed at 145 °C and 15 MPa for 30 min to give sheets with a thickness of ~1 mm.

Dissolution study of cross-linked samples

The cross-linked sheets were cut into disc-shaped specimens with a diameter of 8.0 mm. The cut samples were immersed in

10 mL of toluene/dichloroacetic acid (v/v = 95/5)[31] and kept at room temperature for 4 days, followed by heating (80 °C for 6 h).

Preparation of T-peel test samples

Two sheets of each of the prepared cross-linked rubber samples were attached to each other without any pretreatment or adhesive (Fig. 2; left). To ensure a sufficient gripping area on the specimens for T-peel tests, a thin piece of poly (tetrafluoroethylene) (PTFE) film (length: 15–20 mm) was placed between the two sheets at the edge of the specimens (Fig. 2; middle and right). Then, the laminates were hot-pressed at 145 °C under 15 MPa for 30 min to give specimens of approximately 2 mm.

Results and discussion

Preparation of DPT–SBRs and a small model molecule (DPT-CO)

To prepare the DPT–SBRs, DPT and SBR were kneaded using an internal mixer. After the kneading process, the reaction between red DPT and colourless SBR was visually confirmed to have proceeded by the disappearance of the red colour of DPT and the appearance of a yellow colour (Fig. 3).

For a detailed DPT–SBR characterization, a small model molecule (DPT-CO) was synthesized for comparison. DPT-CO was obtained from the IEDDA reaction between *cis*-cyclooctene and DPT (Scheme 1). Compared to previously reported synthesis conditions, which use *trans*-cyclooctene in THF at room temperature to reach completion immediately,[57] a much higher temperature was required for the reaction with *cis*-cyclooctene, most likely due to its lower strain energy compared to that of *trans*-cyclooctene.[69] Nevertheless, the targeted DPT-CO was obtained in 96% yield.

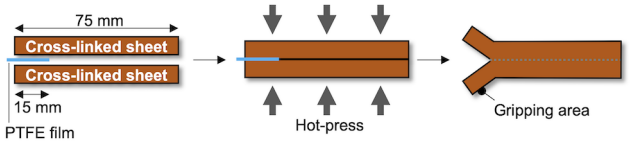

Fig. 2 Schematic description of the preparation of the T-peel test specimens.

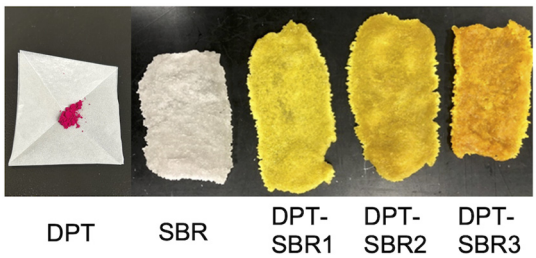

Fig. 3 Photographs of the DPT, SBR and DPT–SBR samples.

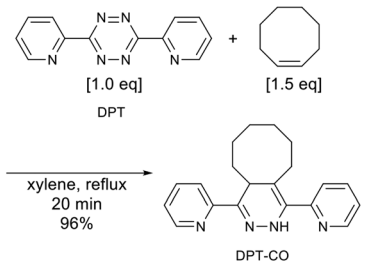

Scheme 1 Synthesis of DPT-CO from DPT and *cis*-cyclooctene.

Characterization of SBR and DPT–SBRs

To characterize the original SBR and obtained DPT–SBRs, ^{1}H NMR, GPC and DSC measurements were carried out and the characteristic values are summarized in Table 1. ^{1}H NMR measurements were performed to characterize the obtained DPT–SBRs in detail (Fig. 4 and Fig. S1 as well as Table S1†). The initial signals for DPT disappeared in the spectrum of the DPT–SBR samples, and new distinctive signals corresponding to the aromatic protons in the DPT unit in the aromatic region and C–H protons (a) at δ 4.33 ppm appeared. In a previous

Table 1 Characterization of SBR and DPT–SBRs

Polymer	Butadiene (1,4 unit : 1,2 unit) : styrene : DPT[a] (mol%)	M_n[b]	M_w/M_n[b]	T_g[c] (°C)
SBR	85.7 (77.3 : 8.4) : 14.3 : —	141 606	2.45	−68.4
DPT–SBR1	84.7 (76.6 : 8.1) : 14.6 : 0.7	81 800	1.78	−65.1
DPT–SBR2	83.6 (75.9 : 7.7) : 15.1 : 1.3	75 096	1.76	−53.5
DPT–SBR3	81.7 (74.1 : 7.6) : 15.7 : 2.6	60 303	1.76	−52.0

[a] Determined by ^{1}H NMR spectroscopy. [b] Determined by GPC based on polystyrene standards (eluent: THF). [c] Determined by DSC.

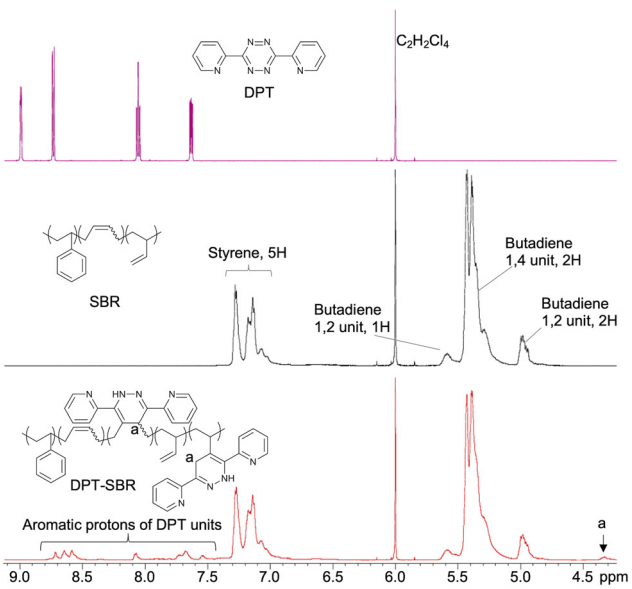

Fig. 4 ^{1}H NMR spectra of DPT, SBR and DPT–SBR3.

study,[55] the signal at 4.33 ppm was assigned to the N–H protons of the DPT units, but this interpretation contradicts the assignment of the ^{1}H NMR spectrum for a DPT unit in a model small molecule (DPT-CO), which was supported by several NMR techniques, including 2D NMR experiments (Fig. S2–S5†). A comparison of the NMR spectra of the DPT–SBR samples with those of DPT-CO suggested that the signal at δ 4.33 ppm for the DPT–SBRs should be assigned to the C–H proton (a) of the DPT units. A close observation of the signals of the butadiene units (δ 5.70–4.70 ppm) revealed that both the content of 1,4 and 1,2 units per mole SBR decrease upon DPT loading, indicating that DPT reacts with both units in the butadiene segments. The modification-efficiency was calculated based on the ratio of the aromatic protons of the DPT units (8H, δ 8.81–7.46 ppm) relative to the aromatic protons of the styrene units in the SBR as well as the protons of the of butadiene 1,4 unit (2H) and the butadiene 1,2 unit (3H, 5.70–4.70 ppm) (eqn (S1)–(S6)†). In their entirety, these results indicate modification-efficiency values of 75.7, 76.4 and 75.8% for DPT–SBR1, DPT–SBR2 and DPT–SBR3, respectively. The unreacted residual DPT in each sample was considered to have further reacted with the SBR during the subsequent curing process and increased the modification efficiency.[55]

The M_n and M_w/M_n values of the SBR and DPT–SBR samples were determined using GPC. The M_n values of the resulting DPT–SBR samples were lower than those of the starting SBR samples (Fig. 5a). The decrease in M_n upon DPT modification is most likely predominantly due to the main-chain scission caused by the oxidative decomposition of the DPT units[70] induced by heat and/or mechanical shear forces[71] during the kneading process. Furthermore, in the GPC profiles monitored using a UV detector, the measured peak intensities of the DPT–SBR samples increased with increasing loading amount of DPT, while the peak intensities measured using an RI detector decreased slightly compared to the unmodified SBR. The increased UV absorbance intensity in the GPC measurements is consistent with the strong UV absorbance of the DPT unit (Fig. S6†), which suggests that the degree of DPT incorporation into the SBR is increased by increasing the amount of DPT used. DSC measurements were performed to determine the glass-transition temperature (T_g) of the samples, and the obtained T_g values of the unmodified SBR, DPT–SBR1, DPT–SBR2 and DPT–SBR3 are −68.4, −65.1, −53.5 and −52.0 °C, respectively (Fig. 5b). The increase in T_g with increased DPT loading is probably due to a decrease in polymer-chain mobility[72] upon incorporation of the bulky DPT units, indicating the successful modification of the SBR with DPT.[55] The DPT-modification of SBR is also supported by FT-IR spectroscopy, in which the distinctive absorbance of the –C═N bending vibration[55] is observed at 1586 cm^{-1}. The intensity of this peak increases with increasing DPT loading (Fig. 5c) and almost identical absorption peaks were observed for the original DPT-CO (Fig. S7†).

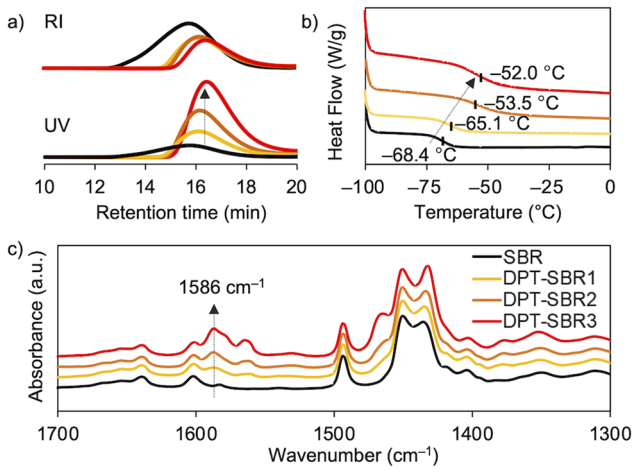

Fig. 5 Characterization of SBR (black), DPT–SBR1 (yellow), DPT–SBR2 (orange) and DPT–SBR3 (red): (a) GPC curves obtained using an RI detector (top) or UV detector (bottom), (b) DSC curves and (c) ATR FT-IR spectra.

ZDMA complexation study

UV-vis measurements were conducted in order to examine the complexation capability of the DPT units in the SBRs with ZDMA, as well as the complexation of DPT-CO with ZDMA. The UV-vis measurements were performed using DPT–SBR3 or DPT-CO in CH_2Cl_2 with a constant DPT-unit concentration of 6.4×10^{-5} M and a gradually varying molar ratio of ZDMA to DPT units from 0 to 2.0 (Fig. 6). Distinctive absorbances at approximately 380 and 450 nm appeared with increasing ZDMA ratio for both DPT–SBR3 and DPT-CO. The latter absorbance is presumably due to the complexation of one DPT unit to a Zn^{2+} ion, given that this absorbance appeared strongly in the presence of an excess of ZDMA relative to the DPT unit. On the other hand, the absorbance at approximately 380 nm appeared first, suggesting that it is due to complexation of two or more DPT units to a Zn^{2+} ion. Furthermore, TOF-MS study using the mixture of DPT-CO and ZDMA was also performed and demonstrated the formation of a complex consisting of a Zn^{2+} ion coordinated to two DPT-CO ligands (Fig. S8†).

Preparation of cross-linked rubber samples

In the next step, cross-linked rubber composites were prepared using unmodified SBR or DPT–SBR samples; the formulation of all samples is summarized in Table 2 and Table S2.† To achieve cross-linking in the unmodified SBR as a control sample, 40 phr of ZDMA and 0.2 phr of dicumyl peroxide (DCP) were mixed (run 1). The control samples with varying degrees of cross-linking density were also prepared by mixing the unmodified SBR with 40 phr of ZDMA and 0.05 or 0.4 phr of DCP (runs S1 and S2†). The samples for runs 2, 3 and 4 were prepared using 40 phr of ZDMA with DPT–SBR1, DPT–SBR2 and DPT–SBR3, respectively, in order to clarify the effects of the amount of bound DPT in the SBR on the physical properties. Further samples were synthesized using 30, 50 and 60 phr of ZDMA, in order to gain further insight into the impact of the amount of incorporated ZDMA on the mechanical behaviour (runs 5, 6 and 7). All samples were mixed with

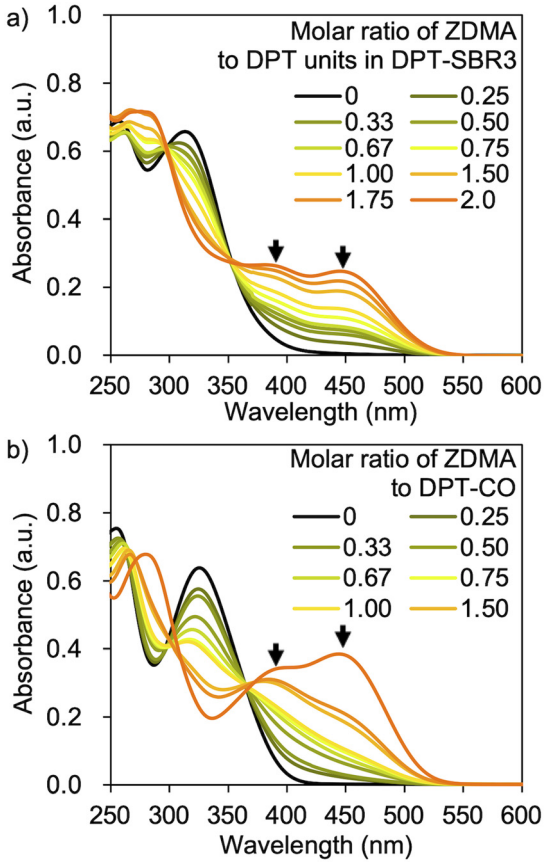

Fig. 6 UV-vis spectra for (a) DPT–SBR3 with ZDMA and (b) DPT-CO with ZDMA.

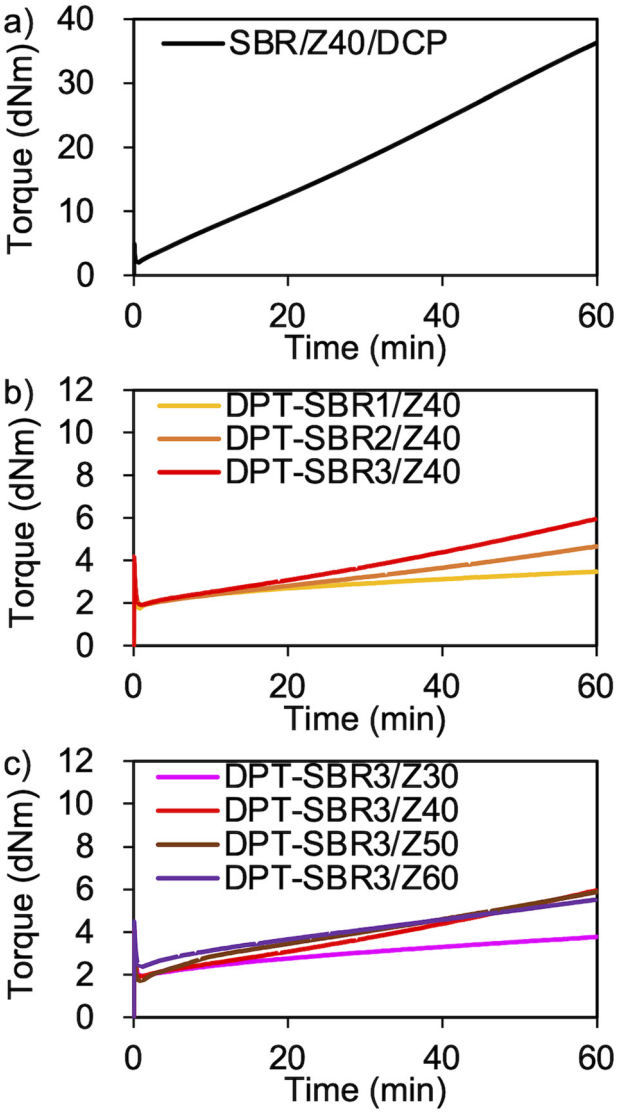

Fig. 7 Elastic torque curves of rubber composites measured using a moving die rheometer at 145 °C: (a) control sample (SBR/Z40/DCP), (b) effect of the amount of bound DPT in the SBRs and (c) effect of the ZDMA content.

an open roll and hot-pressed with an ordinary condition (145 °C; 30 min) into sheets with an approximate thickness of 1 mm. The hot-pressing condition was set to adjust the cross-linking density indicated by the swelling experiment using *n*-heptane of SBR/Z40/DCP and DPT–SBR2/Z40 within the comparable level (Fig. S9†).

Demonstration of DPT/ZDMA cross-linking

To demonstrate the successful cross-linking of DPT–ZDMA, the elastic torque of the samples was analysed using a rheometer at 145 °C (Fig. 7 and S10†). As shown in Fig. 7a, the control SBR sample using DCP based on a conventional peroxide and ZDMA-based curing system showed a rapid and significant increase in its elastic torque.[63] In Fig. 7b, the increase in the elastic torque observed for the DPT–SBR samples loaded with 40 phr of ZDMA indicates the formation of a cross-linking network due to the complexation of DPT with ZDMA. With increasing amount of bound DPT in the SBR

Table 2 Formulation of prepared cross-linked samples. The unit of the values (phr) refers to weight fraction of the specified rubber component per 100 units of the base rubber

Run	1	2	3	4	5	6	7
Sample code	SBR/Z40/DCP	DPT–SBR1/Z40	DPT–SBR2/Z40	DPT–SBR3/Z40	DPT–SBR3/Z30	DPT–SBR3/Z50	DPT–SBR3/Z60
SBR	100						
DPT–SBR1		100					
DPT–SBR2			100				
DPT–SBR3				100	100	100	100
ZDMA	40	40	40	40	30	50	60
DCP	0.2						

samples, the elastic torque increased, suggesting that a higher degree of DPT–ZDMA cross-linking was achieved. The enhanced DPT–ZDMA cross-linking density was confirmed through a swelling experiment with *n*-heptane, which revealed that the swelling degrees of DPT–SBR1/Z40, DPT–SBR2/Z40 and DPT–SBR3/Z40 are consistent with the order of their torque values (Fig. S11†). In Fig. 7c, the impact of ZDMA loading on the elastic torque is presented using DPT–SBR3. The maximum torque for the sample with a 30 phr ZDMA loading is significantly decreased compared to those of the other DPT–SBR3 composites, indicating a lower degree of DPT–ZDMA complexation. On the other hand, the DPT–SBR3 samples with 50 and 60 phr of ZDMA show slightly higher torque values than DPT–SBR3/Z40 at the initial stage of the test, albeit that the maximum torque values are almost the same for these samples. These results suggest that DPT–SBR3/Z40, DPT–SBR3/Z50 and DPT–SBR3/Z60 has almost the same degree of DPT/ZDMA cross-linking at 145 °C.

To further examine the formation of DPT–ZDMA cross-linkages, dissolution and swelling tests were conducted for all composites using toluene/dichloroacetic acid (v/v = 95/5) referring to a previous study[31] (Fig. 8). For that purpose, disc-shaped specimens with a diameter of 8.0 mm (Fig. 8a) were immersed in the solvent (Fig. 8b) and kept at room temperature for 4 days (Fig. 8c). At that point, the solutions of the DPT–ZDMA cross-linked samples turned yellow, indicating that some fraction of the DPT–ZDMA cross-links were dissociated by the acid. Especially DPT–SBR1/Z40 was completely dissolved, while the other DPT–ZDMA cross-linked samples remained partially undissolved, suggesting that the DPT–ZDMA cross-linking density of DPT–SBR1/Z40 is lower than that of the other samples. These samples were further treated at 80 °C for 6 h, which resulted in complete dissolution of all DPT–ZDMA cross-linked samples (Fig. 8d). Interestingly, SBR/Z40/DCP did not show dissolution behaviour, but exhibited swelling instead. These results demonstrate that the SBR/Z40/DCP contains direct C–C covalent cross-links among the SBR main chains, while the DPT–SBRs with ZDMA composites without DCP are formed mainly by DPT–ZDMA coordination cross-linking.

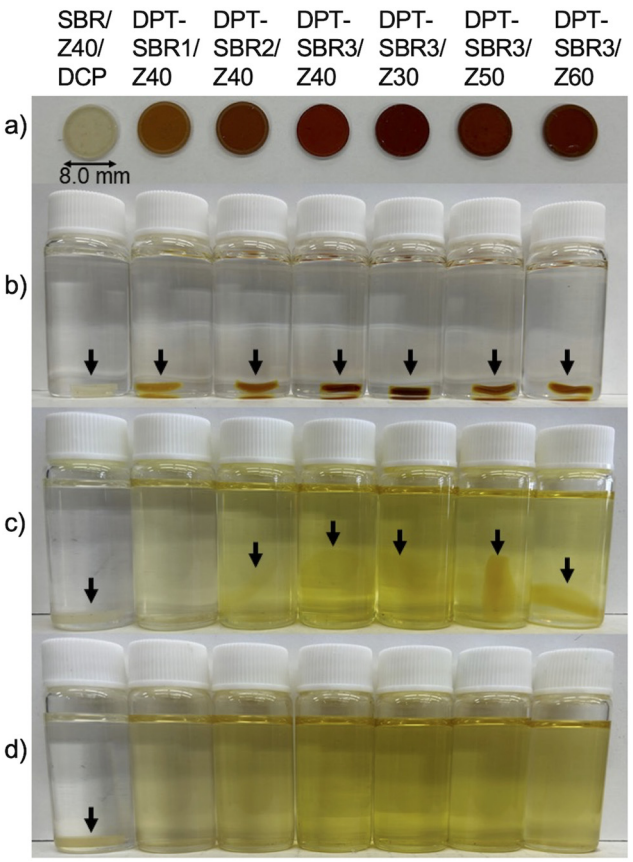

Fig. 8 Photographs documenting the dissolution and swelling behaviour of the cured rubber composites in toluene/dichloroacetic acid (v/v = 95/5): (a) prepared specimens, (b) beginning of the test, (c) after soaking at room temperature for 4 days and (d) after further treatment at 80 °C for 6 h.

DMA measurements

To investigate the temperature dependence of the prepared samples, temperature-sweep DMA tests were carried out at temperatures ranging from −75 to 150 °C (Fig. 9). In Fig. 9a and b, the effects of the amount of bound DPT in the SBRs on E' and tan δ are described. The results show that decrease in E' induced upon raising the testing temperature becomes slower with increasing the amount of bound DPT in the SBRs. Furthermore, the peaks of the tan δ curves due to the glass transition (Fig. S12†) at approximately −40 °C are broader for DPT–SBR2/Z40 and DPT–SBR3/Z40. These results suggest that ZDMA acts as a reinforcing filler and forms bound rubber[73] *via* coordination linkages. Notably, the tan δ curve of SBR-DPT3/Z40 shows a second transition peak at approximately 30 °C. This peak is most likely due to the dynamic dissociation/reassociation of the DPT/ZDMA coordination cross-linkages and ionic multiplets[74] of ZDMA, and possibly including the effect of hydrogen bonding *via* N–H bonds in DPT units with the pyridine groups or the ester groups in ZDMA. The same type of ionic transition peak has been observed in a previous study.[27] In Fig. 9c and d, the impact of the amount of ZDMA on E' and tan δ is described. Upon increasing the ZDMA content from 30 to 60 phr, the shoulders of the E' curves over 0 °C become larger and the peaks in the tan δ curves due to the glass transition become broader, strongly supporting the idea that ZDMA acts not only as a coordination cross-linking point, but also as a reinforcing filler,[73,75] *via* the bound DPT in the SBRs. According to the above discussion, the gap between E' at high and low temperatures seems to reflect the degree of coordination cross-linking, given that the slower decrease in E' observed for the DPT–SBR and ZDMA composites with increasing temperature is most likely due to the dissociation of DPT–ZDMA coordination cross-links. In other words, the difference between the values of E' at high and low temperatures is expected to be a predictor of the degree of DPT–ZDMA cross-linking. As expected, the difference between the values of E' at

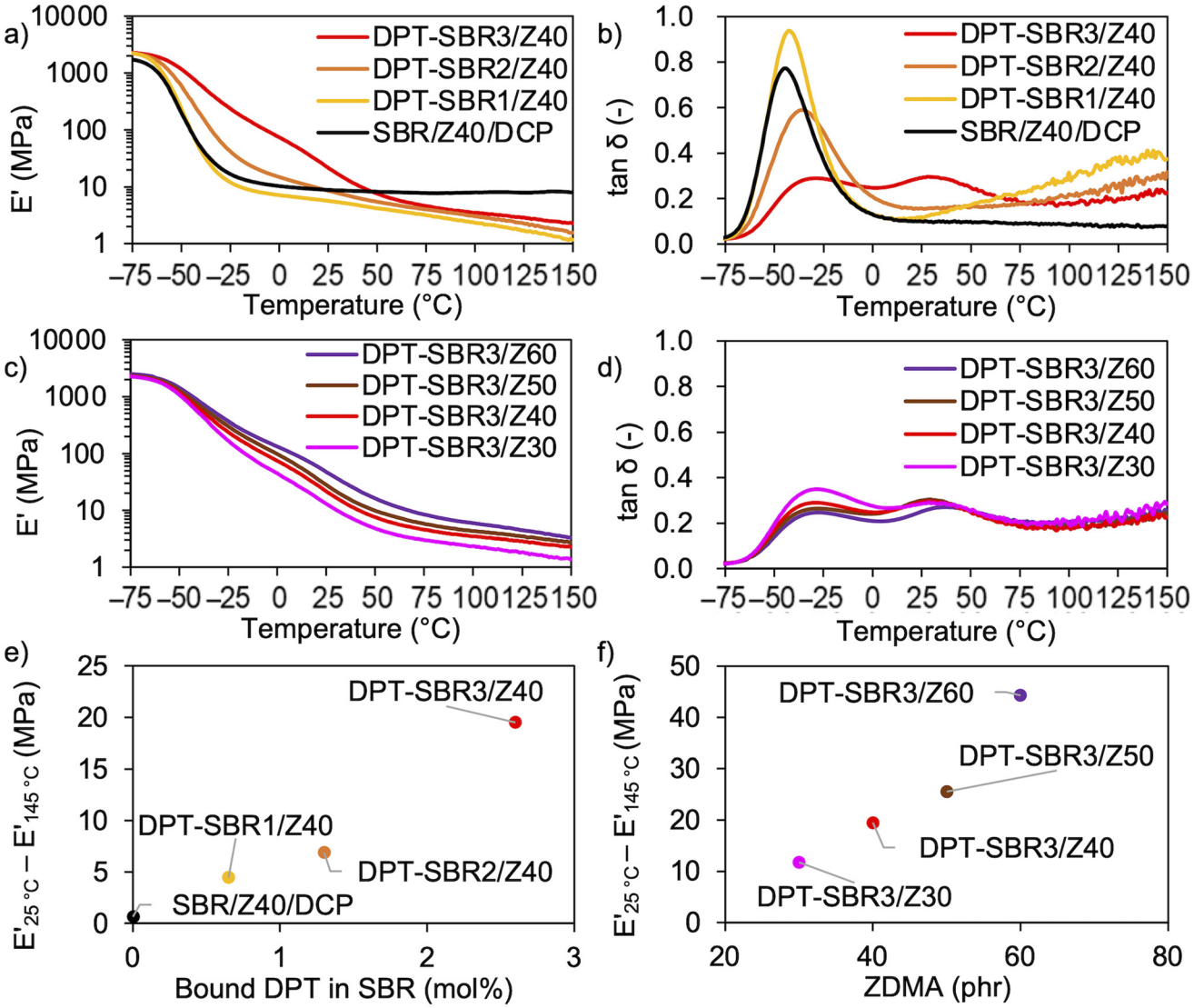

Fig. 9 Temperature dependence of the viscoelasticity: (a) effect of the amount of bound DPT in the SBR on E', (b) effect of the amount of bound DPT in the SBR on tan δ, (c) effect of ZDMA content on E', (d) effect of the loaded ZDMA content on tan δ, (e) effect of the amount of bound DPT in the SBR on the difference between E' at 25 °C and E' at 145 °C and (f) effect of ZDMA content on the difference between E' at 25 °C and E' at 145 °C.

25 °C and 145 °C, denoted as $E'_{25°C} - E'_{145°C}$, shows a good correlation with the degree of bound DPT in the SBRs and the ZDMA loading (Fig. 9e and f). Based on these results, we consider the difference in the value of E' to be a useful tool to interpret the hot-pressed adhesion behaviour, given that the interdiffusion and interlinking behaviour prompted by the dissociation and reassociation of cross-linking are important for hot-pressing adhesion, as mentioned in the introduction.

To further investigate the impact of DPT/ZDMA cross-linking on the dynamic mechanical behaviour, strain-sweep DMA tests were conducted at strains ranging from 0.1 to 10% (Fig. 10). In Fig. 10a, the impact of the amount of bound DPT in the SBRs on the strain dependence of E' are depicted. The control, SBR/Z40/DCP, shows almost no decrease in E' (Payne effect)[76] with increasing strain, indicating that a significant network of ZDMA particles is not formed. On the other hand, DPT–SBR1/Z40 and DPT–SBR2/Z40 show a slight decrease in E' at strains ranging from 5 to 10%, and importantly, DPT–SBR3/Z40 reveals an obvious Payne effect, demonstrating that the bound DPT in the SBRs enhanced the ZDMA–ZDMA filler interaction[66,67] *via* DPT–ZDMA linkages. Fig. 10b depicts the effects of the ZDMA content on the strain dependence of E'; the Payne effect is significantly amplified with increasing ZDMA content, demonstrating that strong ZDMA–ZDMA filler interactions are formed.[65] Based on these results, it seems obvious that ZDMA plays important roles as both a cross-linking point and a reinforcing filler in the DPT–ZDMA cross-linking system.

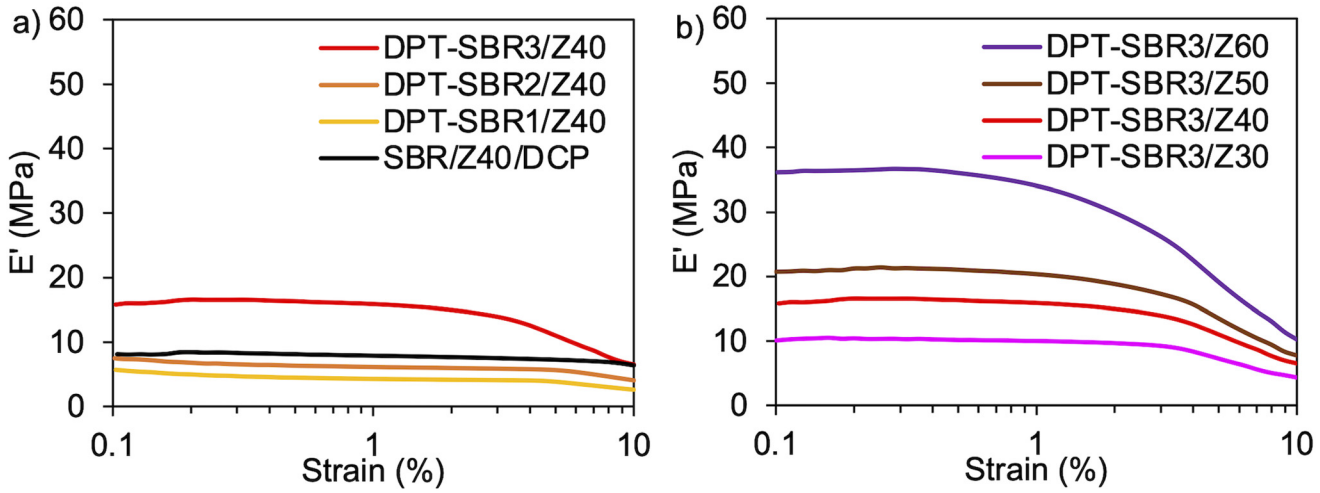

Fig. 10 Strain dependence of E': (a) effect of the amount of bound DPT in the SBR on E' and (b) effect of loaded ZDMA content on E'.

Tensile-test and hysteresis-test results

To investigate the impact of the DPT/ZDMA linkages on the mechanical strength, tensile tests were conducted, and engineering stress–strain curves were obtained (Fig. 11 and S13†); the mechanical properties are summarized in Table 3 and Table S3.† In Fig. 11a, the effect of the amount of bound DPT in the SBRs on the stress–strain curve is depicted. While the control SBR/Z40/DCP shows a relatively low elongation at break (E_b) of 365%, the DPT–SBR composites with 40 phr of ZDMA, DPT–SBR1/Z40, DPT–SBR2/Z40 and DPT–SBR3/Z40, give higher E_b values of 1048, 746 and 512%, respectively. Furthermore, the tensile strength at break (T_b) and the fracture energy of the DPT–SBR composites increases significantly with increasing amount of bound DPT in the SBRs, providing T_b values of 3.99, 9.50 and 30.5 MPa for DPT–SBR1/Z40, DPT–SBR2/Z40 and DPT–SBR3/Z40, respectively. The values of fracture energy of each DPT–SBR composite are higher than the control samples with varying cross-linking density indicated by swelling rate (Fig. S14†). Notably, the T_b value of DPT–SBR3/Z40 is higher than previous reported studies using SBRs with ligand–metal coordination systems.[52,55] The dramatically improved T_b of DPT–SBR3/Z40 is appears to be derived from the strong reinforcement by ZDMA, which is consistent with the results of the DMA measurements. This interpretation is supported by the well-known fact that composites of ZDMA with nitrile–butadiene rubber (NBR) or hydrogenated nitrile–butadiene rubber (HNBR) show high T_b values due to strong reinforcement by ZDMA *via* coordination of the nitrile groups.[63,67] In Fig. 11b, the impact of the level of ZDMA loading on the stress–strain curve is summarized; T_b values of 14.5, 30.5, 29.1 and 25.6 MPa were found for DPT–SBR3/Z30, DPT–SBR3/Z40, DPT–SBR3/Z50 and DPT–SBR3/Z60, respectively, indicating that 40–50 phr is the optimum ZDMA content in terms of tensile strength in this study. The decrease of the T_b of DPT–SBR3/Z30 in comparison with that of DPT–SBR3/Z40 is drastic, which suggests that 30 phr of ZDMA is insufficient to form a ZDMA-reinforced network *via* the bound DPT in the SBR. In contrast, DPT–SBR3/Z50 and DPT–SBR3/Z60 show higher moduli than DPT–SBR3/Z40 over a wide strain range, while the T_b values of DPT–SBR3/Z60 decreased. The increased moduli indicate an increased cross-linking density due to more efficient DPT–ZDMA coordination in addition to the conventional filler-induced hydrodynamic effects and

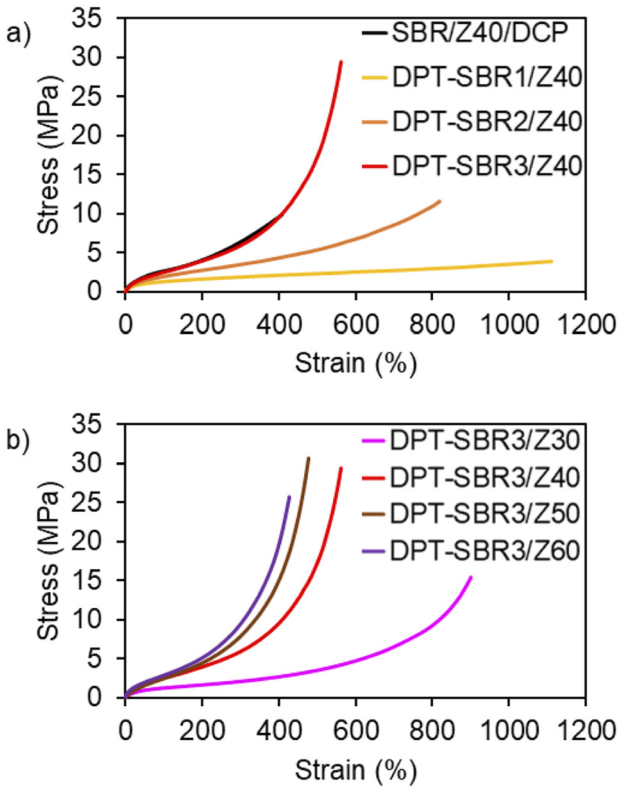

Fig. 11 Engineering stress–strain curves: (a) effect of the amount of bound DPT in the SBRs and (b) effect of loaded ZDMA content.

Table 3 Moduli and fracture parameters of the cross-linked samples shown in Fig. 12. Values in parentheses refer to the standard deviation

Run/sample code	Tensile stress at 100% elongation (MPa)	Tensile stress at 300% elongation (MPa)	Elongation at break (E_b) (%)	Tensile strength at break (T_b) (MPa)	Fracture energy (MJ m^{-3})
1/SBR/Z40/DCP	2.64 (0.03)	6.44 (0.32)	365 (32)	8.50 (0.98)	14.7 (2.91)
2/DPT–SBR1/Z40	1.28 (0.02)	1.89 (0.04)	1048 (46)	3.99 (0.09)	25.2 (0.95)
3/DPT–SBR2/Z40	1.91 (0.01)	3.43 (0.04)	746 (75)	9.50 (1.60)	33.4 (6.01)
4/DPT–SBR3/Z40	2.57 (0.09)	5.83 (0.09)	512 (11)	30.5 (3.01)	46.3 (2.38)
5/DPT–SBR3/Z30	1.25 (0.01)	2.09 (0.03)	893 (4.9)	14.5 (1.31)	36.0 (1.61)
6/DPT–SBR3/Z50	2.62 (0.17)	8.65 (0.97)	455 (24)	29.1 (1.13)	36.0 (2.20)
7/DPT–SBR3/Z60	2.80 (0.07)	10.16 (0.81)	408 (20)	25.6 (0.30)	30.1 (2.26)

strain-amplification effects.[77] The decreased values of T_b for DPT–SBR3/Z60 suggest that excessive loading of ZDMA probably increases the degree of initial flaws.[78]

To further investigate the mechanical strength of the DPT–SBR and ZDMA composites, the strain dependence of the hysteresis loss was determined using hysteresis tests (Fig. 12 and S15†). The effect of the amount of bound DPT in the SBRs and the ZDMA content on the hysteresis loss at 200% as a representative value of hysteresis loss at large strain is summarized in Fig. 13. Fig. 13a shows that the hysteresis loss at 200% strain increases significantly with increasing amount of bound DPT in the SBRs, showing the same trend as the relationship

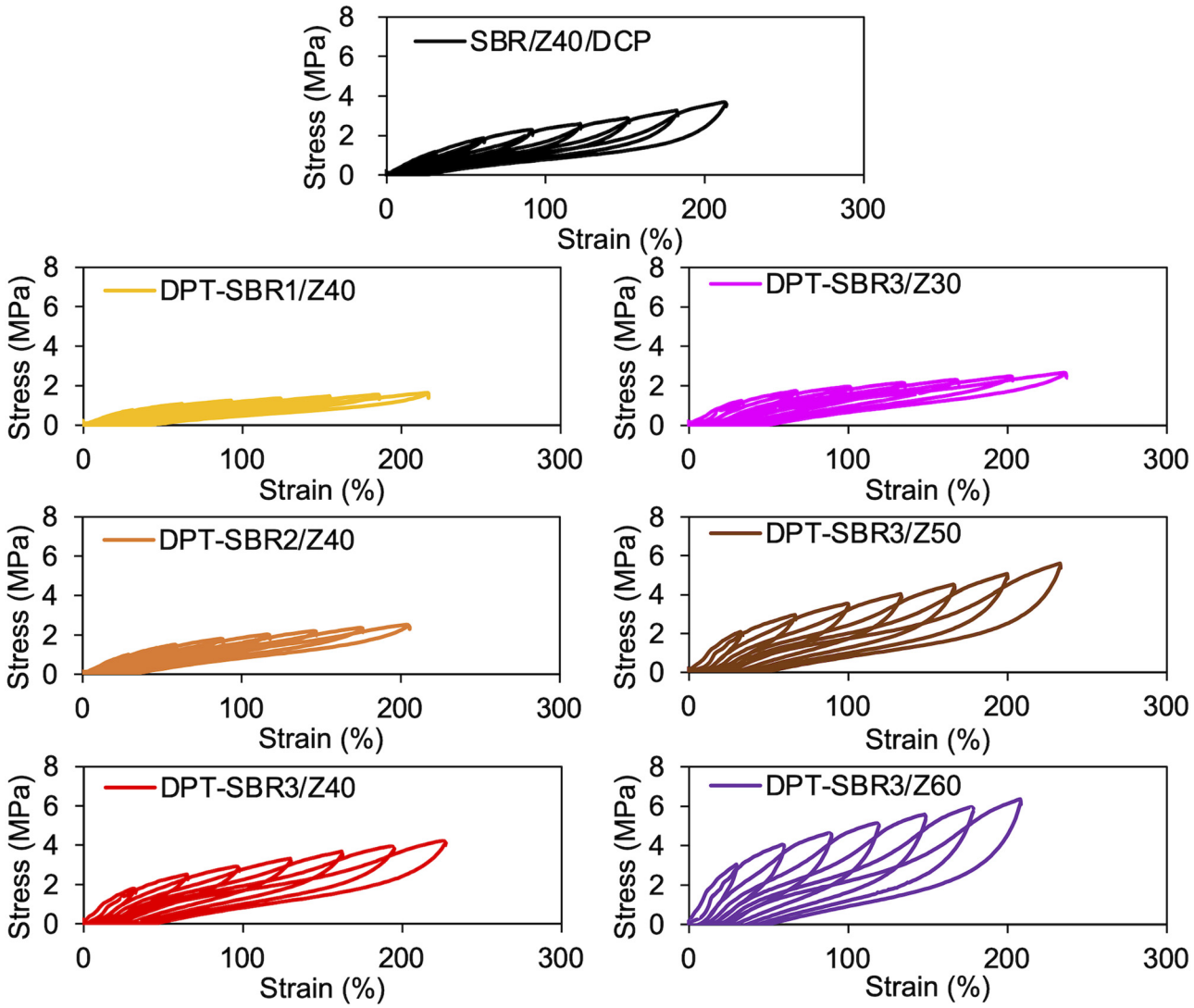

Fig. 12 Hysteresis test results of SBR composites.

between the amount of bound DPT in the SBRs and the T_b values. These results suggest that DPT–ZDMA cross-linking and ZDMA–ZDMA ionic multiplets[74] are dissociated at large strain, accompanied by high energy dissipation, resulting in high T_b values with increasing amount of bound DPT in the SBRs. Notably, DPT–SBR3/Z40 shows comparable hysteresis loss with SBR/Z40/DCP, but the T_b value of the former is much higher than the latter, suggesting that the inherent flaw size[79]

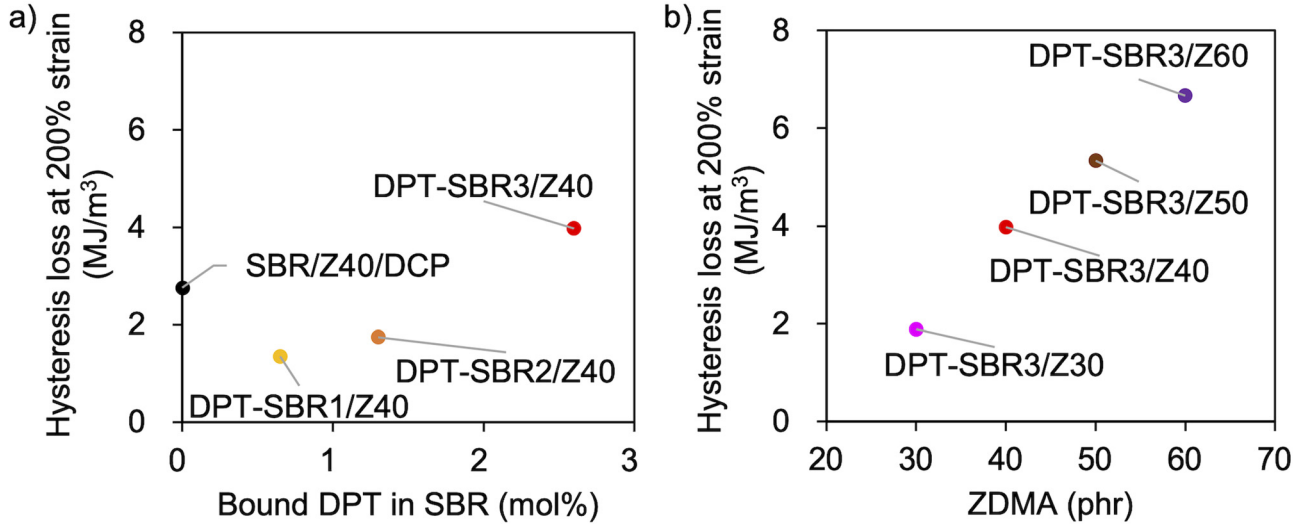

Fig. 13 Hysteresis loss at 200% strain: (a) effect of the amount of bound DPT in the SBR and (b) effect of the amount of loaded ZDMA.

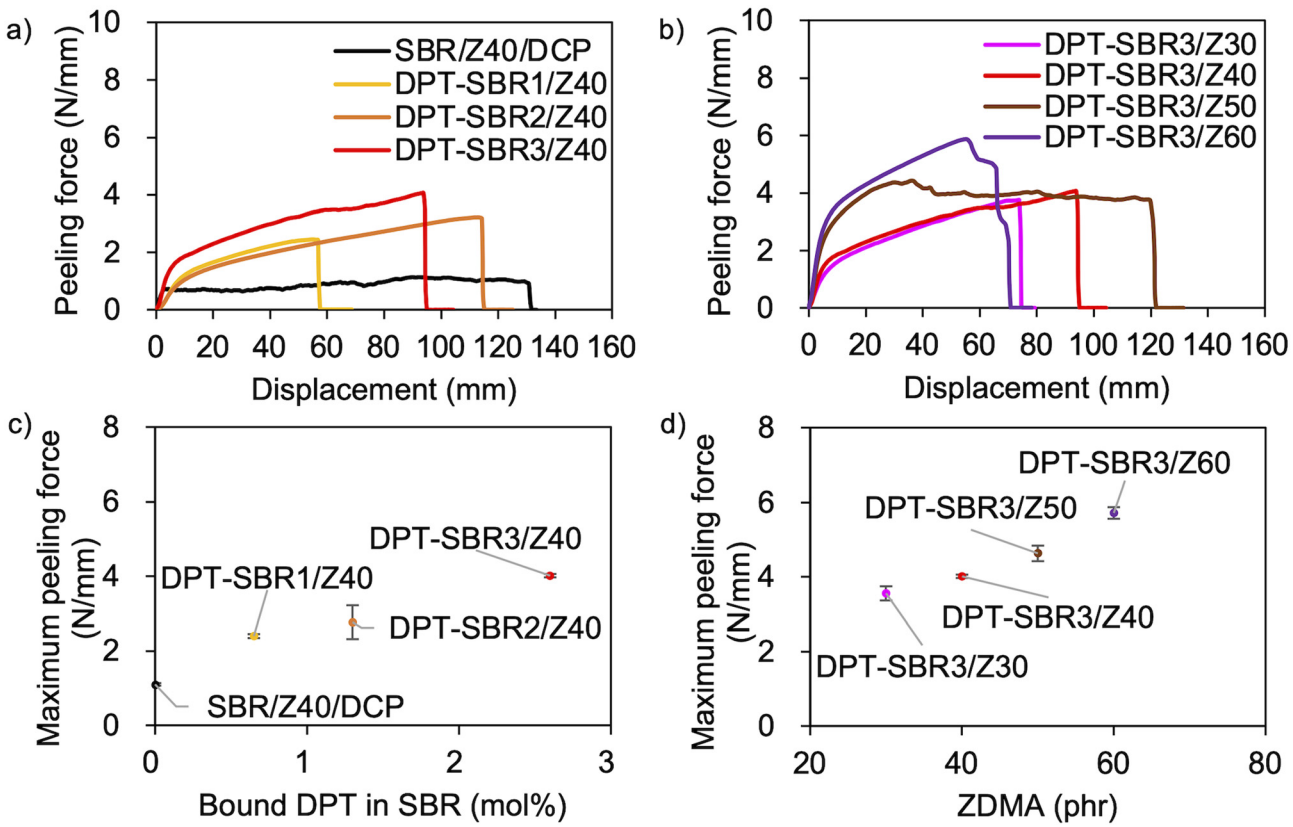

Fig. 14 T-peel test results: (a) effect of the amount of bound DPT in the SBRs, (b) effect of the loaded ZDMA content. Relationship between the maximum peeling force and (c) the amount of bound DPT in the polymer or (d) the loaded ZDMA content.

in the former composite is smaller probably due to the strong reinforcement with ZDMA *via* coordination bonds with DPT units. Fig. 13b presents the impact of the ZDMA content on the hysteresis loss at 200% strain; these values are significantly improved by increasing the ZDMA content. This trend is in line with previous results[67] for NBR and ZDMA composites.

Adhesion performance

The above discussion demonstrates that the DPT–ZDMA cross-links obviously act as reversible bonds, and accordingly, malleability can be expected at high temperatures. Thus, we speculated that the direct adhesion of DPT–ZDMA cross-linked SBRs could be achieved using a hot press. To confirm such a direct adhesion capability, two cross-linked sheets of each sample were stacked and remoulded at 145 °C under 15 MPa for 30 min, before T-peel tests were conducted using the prepared adhered samples (Fig. 14 and S16†). The condition of the adhesion sample preparation was determined by several experimental results with varying temperature and time, and the condition providing the highest adhesion performance was selected (Fig. S17†). Fig. 14a shows the effect of the amount of bound DPT in the SBRs on the peeling force; the composites of DPT–SBR with ZDMA clearly show higher peeling forces than the control sample cured with DCP. Fig. 14b depicts the impact of the ZDMA content on the peeling force; the maximum peeling force values gradually increase with increasing amount of ZDMA. The relationships between the resulting maximum peeling force and the amount of bound DPT in the SBR as well as the ZDMA content are summarized in Fig. 14c and d, respectively. These results demonstrate that the maximum peeling force is dramatically increased with increasing both the amount of bound DPT units in the SBRs and the loaded ZDMA content. Furthermore, the values of maximum peeling force of each DPT–SBR composite are higher than the control samples with varying cross-linking density indicated by swelling rate (Fig. S18†).

In this adhesion process, the degree of DPT–ZDMA cross-linking seems to be one of the most important factors for controlling the adhesion capability. Based on this assumption, the relationship between the maximum peeling force and the predictor of the degree of DPT–ZDMA cross-linking ($E'_{25°C} - E'_{145°C}$) mentioned in the discussion of the temperature sweep DMA results (*vide supra*) was investigated (Fig. 15). The value of the maximum peeling force was found to improve with increasing DPT–ZDMA cross-linking predictor value ($E'_{25°C} - E'_{145°C}$), demonstrating that the direct adhesion strength of the DPT–ZDMA cross-linking system can be explained by the degree of DPT–ZDMA cross-linking.

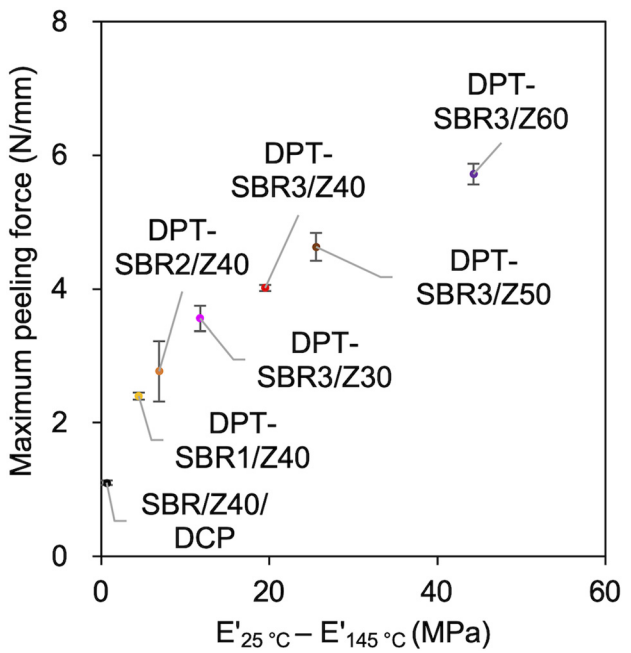

Fig. 15 Relationship between the maximum peeling force and the difference between E' at 25 °C and E' at 145 °C as a predictor of the degree of DPT/ZDMA coordination cross-linking.

Conclusions

To achieve direct adhesion between cross-linked rubbers without any pretreatment of the rubber surfaces or the use of adhesives, we designed novel modified SBR composites that contain zinc dimethacrylate (ZDMA)–nitrogen coordination linkages. These composites were prepared *via* tetrazine click reactions with 3,6-di(2-pyridyl)-1,2,4,5-tetrazine (DPT) during the rubber-kneading process, followed by the addition of ZDMA and a thermal curing process. The DPT modification was confirmed *via* GPC and DSC as well as FT-IR and ^{1}H NMR spectroscopy. The complexation capability of the DPT unit with ZDMA was investigated in detail by conducting a study using a model small molecule (DPT-CO). The UV-vis spectra revealed that both DPT-CO and the DPT units in the SBR showed almost the same absorbance wavelength due to complexation with ZDMA, indicating that similar types of complexation occurred.

In the compounding study, the formation of DPT–ZDMA cross-linking was confirmed by the increase in the elastic torque monitored using a rheometer and the dissolution behaviour in toluene/dichloroacetic acid. The resulting DPT–ZDMA cross-linked SBRs showed a unique decrease in E' and increase in tan δ with increasing temperature in temperature-sweep DMA measurements, most likely due to dynamic dissociation/reassociation of DPT–ZDMA linkages, and the parameter $E'_{25°C} - E'_{145°C}$ was proposed as a predictor of the degree of DPT–ZDMA cross-linking. It was clarified that this predictor value can be controlled by the amount of bound DPT in the SBR and the ZDMA loading amount. Strain-sweep DMA measurements were also carried out, and a typical Payne effect was observed for DPT–ZDMA cross-linked samples, demonstrating that ZDMA plays the role of both cross-linking point and reinforcing filler. Notably, DPT–ZDMA cross-linking also led to unique stress–strain behaviour. Hysteresis tests revealed improved hysteresis loss with a larger amount of bound DPT

in the samples of SBR with ZDMA, resulting in a much higher T_b than that of the conventional peroxide-cured sample. Finally, direct adhesion between cross-linked rubbers was demonstrated, and DPT–ZDMA cross-linked samples showed improved adhesion strength, consistent with the increase in the predictor of the degree of DPT–ZDMA cross-linking ($E'_{25°C} - E'_{145°C}$). In conclusion, we have successfully established a novel system for direct adhesion between cross-linked rubbers. We are convinced that this technology not only represents a new approach to rubber bonding, but can also be expected to contribute to the improvement of rubber repair processes, which would lead to a reduction in CO_2 emissions and rubber waste.

Author contributions

K. K., K. T. and H. O. conceived the concept and designed the experiments. K. K. performed the experiments and analysed the data. K. K., K. T. and H. O. wrote the manuscript.

Conflicts of interest

There are no conflicts to declare.

Acknowledgements

This work was supported by JST-Mirai Program Grant Number JPMJMI18A2, Japan.

References

1 D. K. Kotnee and A. K. Bhowmick, *Rubber to Rubber Adhesion*, Scrivener Publishing LLC, Beverly, 2021.
2 R.-J. Chang and A. N. Gent, *J. Polym. Sci., Polym. Phys. Ed.*, 1981, **19**, 1619–1633.
3 A. K. Bhowmick and A. N. Gent, *Rubber Chem. Technol.*, 1984, **57**, 216–226.
4 H. Chun and A. N. Gent, *J. Polym. Sci., Part B: Polym. Phys.*, 1996, **34**, 2223–2229.
5 F. Ruch, M. O. David and M. F. Vallat, *J. Polym. Sci., Part B: Polym. Phys.*, 2000, **38**, 3189–3199.
6 D. Oldfield and T. E. F. Symes, *J. Adhes.*, 1983, **16**, 77–96.
7 J. M. Martín-Martínez, J. C. Fernández-García, F. Huerta and A. C. Orgilés-Barceló, *Rubber Chem. Technol.*, 1991, **64**, 510–521.
8 M. S. Sánchez-Adsuar, M. M. Pastor-Blas, R. Torregrosa-Maciá and J. M. Martín-Martínez, *Int. J. Adhes. Adhes.*, 1994, **14**, 193–200.
9 M. D. Romero-Sánchez, M. M. Pastor-Blas and J. M. Martín-Martínez, *Int. J. Adhes. Adhes.*, 2001, **21**, 325–337.
10 M. M. Pastor-Blas, J. M. Martín-Martínez and J. G. Dillard, *Surf. Interface Anal.*, 1998, **26**, 385–399.
11 H. Hirahara, K. Mori and Y. Oishi, *J. Adhes. Sci. Technol.*, 1997, **11**, 1459–1474.
12 J. Tyczkowski, I. Krawczyk and B. Wożniak, *Surf. Coat. Technol.*, 2003, **174–175**, 849–853.
13 T. F. Petrova, A. A. Shcherbina and A. E. Chalykh, *Polym. Sci., Ser. C*, 2007, **49**, 89–94.
14 S. Nakane, *Nippon Gomu Kyokaishi*, 2012, **85**, 204–207.
15 Indriasari, J. Noordermeer and W. Dierkes, *Appl. Sci.*, 2021, **11**, 9834.
16 G. Ferrer, *Resour., Conserv. Recycl.*, 1997, **19**, 221–255.
17 D. Dobrotă, G. Dobrotă and T. Dobrescu, *J. Cleaner Prod.*, 2020, **260**, 121141.
18 J. Gaidhane, I. Ullah and A. Khalatkar, *Mater. Today: Proc.*, 2022, **60**, 2257–2261.
19 P. K. Behera, S. Mohanty and V. K. Gupta, *Polym. Chem.*, 2021, **12**, 1598–1621.
20 J. Xu, L. Zhu, Y. Nie, Y. Li, S. Wei, X. Chen, W. Zhao and S. Yan, *Materials*, 2022, **15**, 5993.
21 B. Li, P.-F. Cao, T. Saito and A. P. Sokolov, *Chem. Rev.*, 2023, **123**, 701–735.
22 M. Das, A. R. Parathodika, P. Maji and K. Naskar, *Eur. Polym. J.*, 2023, **186**, 111844.
23 K. Chino and M. Ashiura, *Macromolecules*, 2001, **34**, 9201–9204.
24 C.-C. Peng and V. A. Abetz, *Macromolecules*, 2005, **38**, 5575–5580.
25 J. Liu, S. Wang, Z. Tang, J. Huang, B. Guo and G. Huang, *Macromolecules*, 2016, **49**, 8593–8604.
26 Y. Shoda, D. Aoki, K. Tsunoda and H. Otsuka, *Polymer*, 2020, **202**, 122700.
27 I. Mora-Barrantes, M. A. Malmierca, J. L. Valentin, A. Rodriguez and L. Ibarra, *Soft Matter*, 2012, **8**, 5201–5213.
28 A. Das, A. Sallat, F. Böhme, M. Suckow, D. Basu, S. Wießner, K. W. Stöckelhuber, B. Voit and G. Heinrich, *ACS Appl. Mater. Interfaces*, 2015, **7**, 20623–20630.
29 C. Xu, L. Cao, X. Huang, Y. Chen, B. Lin and L. Fu, *ACS Appl. Mater. Interfaces*, 2017, **9**, 29363–29373.
30 Y. Miwa, J. Kurachi, Y. Kohbara and S. Kutsumizu, *Commun. Chem.*, 2018, **1**, 5.
31 C. Li, Z. Yuan and L. Ye, *Composites, Part A*, 2019, **126**, 105580.
32 J. Liu, C. Xiao, J. Tang, Y. Liu and J. Hua, *Ind. Eng. Chem. Res.*, 2020, **59**, 12755–12765.
33 A. M. Wemyss, A. Marathianos, E. L. Heeley, J. Ekeocha, Y. Morishita, R. di Ronza, M. M. Bernal, D. M. Haddleton and C. Wan, *ACS Appl. Polym. Mater.*, 2022, **4**, 7868–7877.
34 A. Harada, Y. Takashima and M. Nakahata, *Acc. Chem. Res.*, 2014, **47**, 2128–2140.
35 G. Sinawang, M. Osaki, Y. Takashima, H. Yamaguchi and A. Harada, *Chem. Commun.*, 2020, **56**, 4381–4395.
36 C. J. Kloxin and C. N. Bowman, *Chem. Soc. Rev.*, 2013, **42**, 7161–7173.
37 N. V. Herck and F. E. Du Prez, *Macromolecules*, 2018, **51**, 3405–3414.
38 P. Tanasi, M. Hernández Santana, J. Carretero-González, R. Verdejo and M. A. López-Manchado, *Polymer*, 2019, **175**, 15–24.

39 A. L. Dobson, N. J. Bongiardina and C. N. Bowman, *ACS Appl. Polym. Mater.*, 2020, **2**, 1053–1060.
40 B. T. Michal, E. J. Spencer and S. J. Rowan, *ACS Appl. Mater. Interfaces*, 2016, **8**, 11041–11049.
41 L. M. Polgar, M. van Duin, A. A. Broekhuis and F. Picchioni, *Macromolecules*, 2015, **48**, 7096–7105.
42 A. Takahashi, R. Goseki, K. Ito and H. Otsuka, *ACS Macro Lett.*, 2017, **6**, 1280–1284.
43 A. Tsuruoka, A. Takahashi, D. Aoki and H. Otsuka, *Angew. Chem., Int. Ed.*, 2020, **59**, 4294–4298.
44 S. Kataoka, A. Tsuruoka, D. Aoki and H. Otsuka, *ACS Appl. Polym. Mater.*, 2021, **3**, 888–895.
45 L. L. Robinson, E. S. Taddese, J. L. Self, C. M. Bates, J. R. de Alaniz, Z. Geng and C. J. Hawker, *Macromolecules*, 2022, **55**, 9780–9789.
46 D. Mozhdehi, S. Ayala, O. R. Cromwell and Z. Guan, *J. Am. Chem. Soc.*, 2014, **136**, 16128–16131.
47 C.-H. Li, C. Wang, C. Keplinger, J.-L. Zuo, L. Jin, Y. Sun, P. Zheng, Y. Cao, F. Lissel, C. Linder, X.-Z. You and Z. A. Bao, *Nat. Chem.*, 2016, **8**, 618–624.
48 X. Zhang, Z. Tang, B. Guo and L. Zhang, *ACS Appl. Mater. Interfaces*, 2016, **8**, 32520–32527.
49 Y.-L. Rao, A. Chortos, R. Pfattner, F. Lissel, Y.-C. Chiu, V. Feig, J. Xu, T. Kurosawa, X. Gu, C. Wang, M. He, J. W. Chung and Z. Bao, *J. Am. Chem. Soc.*, 2016, **138**, 6020–6027.
50 Z. Tang, J. Huang, B. Guo, L. Zhang and F. Liu, *Macromolecules*, 2016, **49**, 1781–1789.
51 M. Das, S. Pal and K. Naskar, *eXPRESS Polym. Lett.*, 2020, **14**, 860–880.
52 M. Mareliati, L. Tadiello, S. Guerra, L. Giannini, S. Schrettl and C. Weder, *Macromolecules*, 2022, **55**, 5164–5175.
53 S. Mandal, F. Simon, S. S. Banerjee, L. B. Tunnicliffe, C. Nakason, C. Das, M. Das, K. Naskar, S. Wiessner, G. Heinrich and A. Das, *ACS Appl. Polym. Mater.*, 2021, **3**, 1190–1202.
54 Q. Wang, Y. Shi, Q. Li and C. Wu, *Eur. Polym. J.*, 2021, **150**, 110415.
55 Q. Wang, W. Wang, Q. Li and C. Wu, *Ind. Eng. Chem. Res.*, 2021, **60**, 2163–2177.
56 H. C. Kolb, M. G. Finn and K. B. Sharpless, *Angew. Chem., Int. Ed.*, 2001, **40**, 2004–2021.
57 M. L. Blackman, M. Royzen and J. M. Fox, *J. Am. Chem. Soc.*, 2008, **130**, 13518–13519.
58 N. K. Devaraj and R. Weissleder, *Acc. Chem. Res.*, 2011, **44**, 816–827.
59 K. Kang, J. Park and E. Kim, *Proteome Sci.*, 2016, **15**, 15.
60 B. L. Oliveira, Z. Guo and G. J. L. Bernardes, *Chem. Soc. Rev.*, 2017, **46**, 4895–4950.
61 I. A. Barker, D. J. Hall, C. F. Hansell, F. E. Du Prez, R. K. O'Reilly and A. P. Dove, *Macromol. Rapid Commun.*, 2011, **32**, 1362–1366.
62 S. Jain, K. Neumann, Y. Zhang, J. Geng and M. Bradley, *Macromolecules*, 2016, **49**, 5438–5443.
63 A. Nomura, J. Takano, A. Toyoda and T. Saito, *Nippon Gomu Kyokaishi*, 1993, **66**, 830–838.
64 R. Costin, W. Nagel and R. Ekwall, *Rubber Chem. Technol.*, 1991, **64**, 152–161.
65 Y. Lu, L. Liu, M. Tian, H. Geng and L. Zhang, *Eur. Polym. J.*, 2005, **41**, 589–598.
66 Y. Chen and C. Xu, *Polym. Compos.*, 2011, **32**, 1593–1600.
67 Y. Chen, C. Xu and Y. Wang, *J. Reinf. Plast. Compos.*, 2012, **31**, 705–716.
68 J. Chen, L. Liao, F. Zhang, S. Hu, J. Huang, S. Shuyun, H. Dongning and X. Mingyue, *Polym. Eng. Sci.*, 2023, **63**, 1388–1400.
69 P. v. R. Schleyer, J. E. Williams and K. R. Blanchard, *J. Am. Chem. Soc.*, 1970, **92**, 2377–2386.
70 F. Karaki, T. Kiguchi, K. Itoh, N. Sato, K. Konishi and H. Fujii, *Tetrahedron*, 2021, **97**, 132411.
71 F. Bueche, *J. Appl. Polym. Sci.*, 1960, **4**, 101–106.
72 E. A. DiMarzio and J. H. Gibbs, *J. Polym. Sci., Part A: Gen. Pap.*, 1963, **1**, 1089–1472.
73 I. Pliskin and N. Tokita, *J. Appl. Polym. Sci.*, 1972, **16**, 473–492.
74 A. Eisenberg, B. Hird and R. B. Moore, *Macromolecules*, 1990, **23**, 4098–4107.
75 Y. Fukahori, *Rubber Chem. Technol.*, 2007, **80**, 701–725.
76 A. R. Payne, *J. Appl. Polym. Sci.*, 1965, **9**, 2273–2284.
77 M. Klüppel and J. Schramm, *Macromol. Theory Simul.*, 2000, **9**, 742–754.
78 A. N. Gent, in *Science and Technology of Rubber*, ed. F. R. Eirich, Academic Press, Inc., New York, 1st edn, 1978, ch. 10, pp. 419–454.
79 G. R. Hamed, *Rubber Chem. Technol.*, 1983, **56**, 244–251.